International Journal of Microwave and Wireless Technologies

cambridge.org/mrf

Design of polarization reconfigurable Koch fractal antenna for S-and C-band applications

Khushbu Patel and Santanu Kumar Behera

Department of Electronics and Communication Engineering, National Institute of Technology, Rourkela, India

Research Paper

Cite this article: Patel K, Behera SK (2024) Design of polarization reconfigurable Koch fractal antenna for S-and C-band applications. *International Journal of Microwave and Wireless Technologies*, 1–14. https://doi.org/10.1017/S1759078724001302

Received: 17 May 2024
Revised: 26 November 2024
Accepted: 29 November 2024

Keywords:
axial ratio bandwidth; fractal patch; miniaturization; PIN diode; reconfiguration; wideband

Corresponding author: Khushbu Patel; Email: khushbupatel869@gmail.com

Abstract

In this research, a novel polarization reconfigurable fractal antenna with high gain is proposed for wideband applications. This antenna consists of a Koch curve based hexagonal ring patch, two Positive-Intrinsic-Negative (PIN) diodes, and partial ground. The patch is positioned on a Rogers RT/Duroid 5880 substrate ($\epsilon r = 2.2$) with overall dimensions $33 \times 30 \times 1.6$ mm3. It has three frequency bands with three different cases i.e., case I, 3–7.91 (90%); case II, 3–7.73 (88.16%); and case III, 3.54–6.7 GHz (61.7%). As a result, the proposed antenna's impedance bandwidth (IBW) offers constant wideband coverage ranging from 3–7.91 GHz (90%). The axial ratio bandwidth (ARBW) is below 3 dB over 3.6–6.9 (62.86%) and 3.33–7.14 GHz (72.78%) for LHCP (Case I) and RHCP modes (Case II), respectively. The value for LP mode (Case III) is 3.54–6.7 GHz (61.7%). A peak realized gains of 4.75, 5.07, and 3.8 dBi are achieved at 6.2, 6.3, and 6 GHz for Case I, Case II, and Case III, respectively. Both linear and circular polarization prototype was developed and the performance was verified through measurements. The design confirms good polarization-reconfigurable characteristics within the band of 3.91 – 7.91 GHz.

Introduction

Reconfigurable fractal antennas (RFAs) [1, 2] have drawn more interest in wireless communication systems develop rapidly because of their ability to reduce noise interference, increase security, expand the radiation coverage area, and more. In simple terms, the antenna's reconfigurable parameters primarily consist of frequency [3–5], polarization [6–15], and radiation pattern [16–19]. Reconfigurable antennas with a single parameter that operate effectively have been thoroughly examined and discussed in the literature [4–15]. Multiple parameter reconfigurable antennas [1–3, 16, 17] that can reconfigure at least two of the three parameters simultaneously are extremely needed for lightweight and versatile communication systems as the communication technology advances. Recently, some reconfigurable antennas have been successfully designed. These include frequency and polarization reconfigurable antennas, frequency and pattern reconfigurable antennas, and polarization with pattern reconfigurable antennas. These antennas have the agility of two of three parameters. However, achieving the agility of all three characteristics is quite difficult. The literature has only reported on a limited number of antennas that have achieved simultaneous reconfiguration of polarization, radiation pattern, and operational frequency [1], and [2]. Antennas realized in literature have the features of both the polarization agility with steerable radiation pattern, frequency with pattern [16, 17] as well as frequency with polarization [3]. There are extremely few known designs for compound reconfigurable antennas (CRAs) [1, 2] that allow reconfiguration of frequency, polarization, and pattern all inside the same geometry. The design structures described in references [14] and [15] may have a variety of reconfigurable working states, but because they make extensive use of PIN diodes, their structural complexity is more and their manufacture is challenging, particularly with regard to the biasing circuitry. Certain CRAs are constructed with fewer diodes and simpler shape reported in references [16] and [17]. Nonetheless, the benefits of circularly polarized (CP) antennas arise from their ability to reduce multipath fading and polarization mismatch brought on by transmitting and receiving antenna orientation mismatch. In [3], researchers investigated on antennas that could be reconfigured in terms of both frequency and polarization. Liquid metal was utilized to implement the reconfigurable frequency and change the polarizations. Multiple numbers of PIN diodes have been used to create polarization reconfigurable antennas with extremely broad operating frequency bandwidths [6–10]. To achieve reconfigurable polarizations in references [11–15], switching elements and variously shaped patches, including square patches with T-shaped feeds, circular patches, U-slotted radiators, C-shaped slots in circular patches, and Koch fractal-based square patches, have been used. These allow

the antennas to be switched between left-hand circular polarization (LHCP) and right-hand circular polarization (RHCP) radiation characteristics. The above radiators change the polarization states through altering the shape of radiators [6–15]. This approach often requires the utilization of a large number of varactors or PIN diodes. As a result, the radiation efficiency would be reduced, the DC-bias circuit would become more complex, and the cost would rise [12], and [13]. Utilizing a switchable feeding network with distinct output phases and magnitudes is another popular method for polarization reconfigurable antennas [14]. In general, complex circuits like phase shifters and couplers are needed for the polarization reconfigurable performance of the majority of reconfigurable feeding networks. That would make the antenna larger and more intricately designed. Further, despite the fact that all of the previously mentioned antennas exhibit good reconfigurable polarization characteristics – such as a wide operating BW or multiple polarization states – very few array applications have been mentioned because of the antennas' large feeding system, complex bias circuits, or radiation element's large footprint. As such, they often have small radiation gain and single element antenna application [16–26].

In this communication, a high-gain, low-complexity hexagonal patch antenna based on the Koch curve fractal with polarization reconfigurability is proposed. The polarization of the designed geometry can be varied between linearly polarized (LP), LHCP, and RHCP by varying the operational states of the switching components in the hexagonal ring. The patch is fed with the microstrip line, which is easy to design. The proposed antenna exhibits good polarization-reconfigurable properties, as demonstrated by the simulated and measured outcomes. The designed antenna's measured common operational bandwidth for three states ranges from 3 to 7.91 GHz. A comparison between the proposed design and existing reconfigurable designs [7–15, 22–24] that have been reported in recent literature is shown in Table 2. Based on the comparison, it can be observed that this antenna has a wider impedance bandwidth (IBW), a wider axial ratio bandwidth (ARBW), and a greater antenna gain.

The article is arranged in the given sections. The "Antenna design geometry" section offers an overview of the fundamentals of RFA topology and design structure. This part shows details of the design technique of creating a Koch curve-based fractal with switching characteristics and the evolution of the proposed design with dimensional parameters. In the "RFA design steps and analysis" section, RFA design steps and parametric study are also described. The "Proposed antenna performance and discussion" section discusses the antenna performance and focuses on the performance comparison of the designed antenna to the existing work. The conclusions are summarized in the "Conclusion" section.

Antenna design geometry

The antenna geometry and dimensions are displayed in Fig. 1. A Rogers RT Duroid 5880 substrate spanning 33 mm × 30 mm × 1.6 mm and having $\varepsilon_r = 2.2$ and tan $\delta = 0.0009$ is used to print the antenna. Relative permittivity of a substrate is an intrinsic property of the material. The dielectric constant of the substrates used for planar antennas varies in the range between $2.2 \leq \varepsilon_r \leq 12$ [27]. As we go up in the range the losses in the antenna increase, whereas when going down the range the losses get minimized and the antenna achieves maximum radiation capability. This maximized radiation gives a relatively good directive gain to the antenna element. The proposed antenna is designed on Rogers RT/Duroid 5880 which has a relative permittivity of ($\varepsilon_r = 2.2$) having low loss. Hence, the realized gain of the proposed antenna gets enhanced and reached to a peak value of 5.07 dBi. The antenna is composed of a partial ground plane with a rectangular shape and a patch with a hexagonal shape. Two 6.5 mm wide triangular extensions (L_g, W_g) are added to the ground plane. From the top edge of the ground plane, a single, rectangular slit approximately 4.5 mm (L_f, W_f) is etched out. By attaching the patch to the feedline, a thin 0.3 mm-wide strip is utilized to achieve reconfigurable characteristics. A 4.5 mm wide, 50 Ω microstrip line is used to feed the antenna, and it is optimized for reconfiguration of polarization. Polarization status and frequency can be adjusted by connecting those smaller rectangular metallic strips individually to the monopole as PIN diodes. This is because the adjustment alters the surface current distribution. The ground initially having a rectangular structure is further modified by adding two triangular-shaped metallic extensions and these are also attached to the ground as shown in Fig. 1(c). On the inside of the hexagonal patch, Koch curve-based fractal geometry is used to increase the bandwidth and provide appropriate impedance matching.

Reconfigurability is achieved by inserting two flip chip MADP 000907-14020x PIN diodes [28], D_1 and D_2, at two 0.3 mm narrow gaps. A resistor of 5.2 Ω in series with an inductor of 0.45 nH is the equivalent circuit of the diode in the ON state shown in Fig. 3. In the off state, a 7 kΩ resistor and a 0.025 pF capacitor are connected in parallel with the inductor [28]. The biasing circuitry, as seen in Fig. 4, consists of two 100 pF capacitors, C_1 and C_2, for dc blocking, and three 250 nH inductors, L_{n1}–L_{n3}, for radio frequency (RF) choking. The values of capacitor and inductor are determined with the help of literature survey [27, 29–32] and component datasheets [28, 33, 34].

RFA design steps and analysis

Fractal generation

Figure 5 displays the fractal structure of the Koch curve. It is a line segment taking parts signified as β. The segment of the part is split into a group of three sub-parts, denoted as β/3. The length of the separated segments of β_1, β_2, and β_3 is $L/3$. Iteration is the term used to describe this continuous repetition of portion division.

The segment is split by a factor of 3 for each iteration of the line L, starting with $L_1 = L/3$, continuing with $L_2 = L/9$ for the 2nd iteration, $L_3 = L/27$ for the 3rd, and so on until the n^{th} iteration. The equations that apply for Koch curve-based structure and iterations to the n^{th} order are (1–3). Equation (4) demonstrates that the Koch curve is $(4/3)^n$ for the entire length of the line segment L. Higher-order iterations of the fractal geometry were not feasible due to the limitations and fabrication difficulties. Thus, the 2nd iteration has been considered the most appropriate iteration of the design in this research endeavor.

$$\beta_1 = L/3 \rightarrow L_1 = 4\beta \tag{1}$$

$$\beta_2 = L/3 \rightarrow L_2 = 16\beta \tag{2}$$

$$\beta_n = L/3 \rightarrow L_n = 4^n\beta_n \tag{3}$$

$$L = (4/3)^n \tag{4}$$

Larger electrical lengths of radiating patches can be carried out inside a specified region by applying fractal curves along the

https://doi.org/10.1017/S1759078724001302 Published online by Cambridge University Press

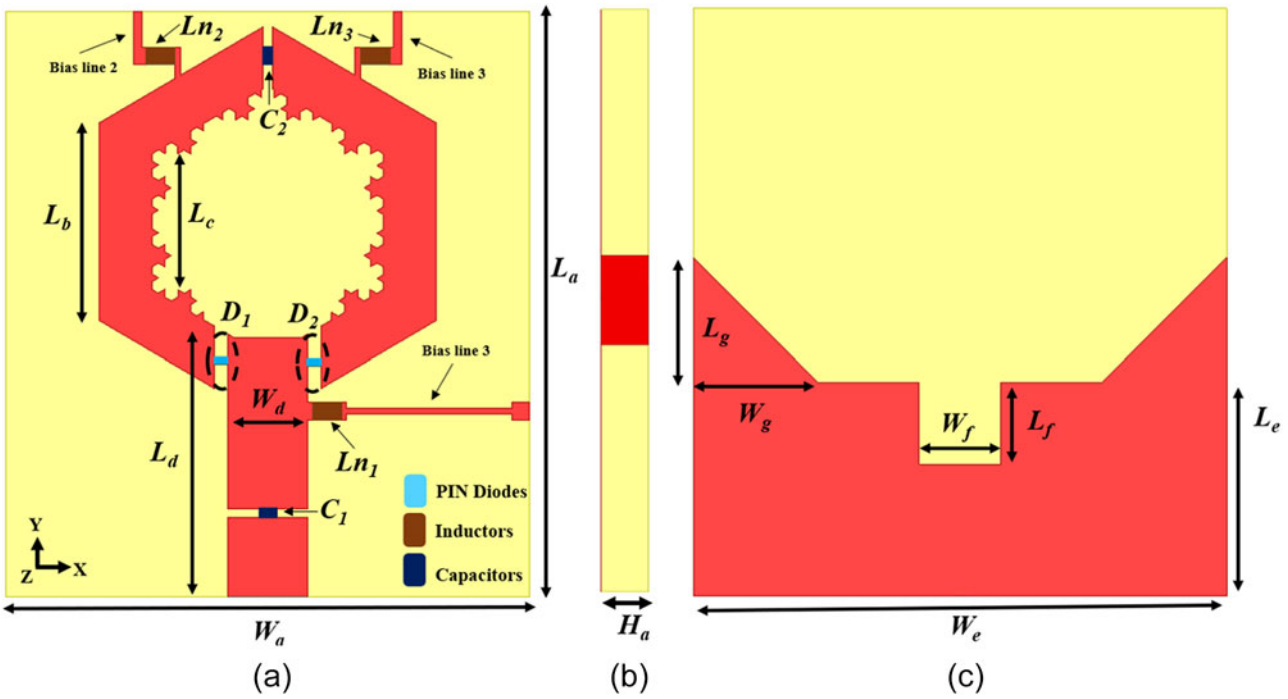

Figure 1. Design overview of reconfigurable fractal antenna. ($W_a = 30$, $L_a = 33$, $H_a = 1.6$, $L_b = 11.5$, $L_c = 7.5$, $W_d = 4.5$, $L_d = 14.5$, $W_e = 30$, $L_e = 12$, $W_g = 6.5$, $L_g = 6.5$, $W_f = 4.5$, $L_f = 4.5$, all dimensions are in millimeters).

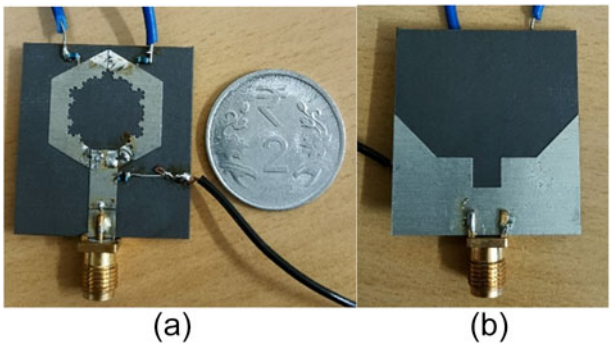

Figure 2. Fabricated prototype of reconfigurable fractal antenna.

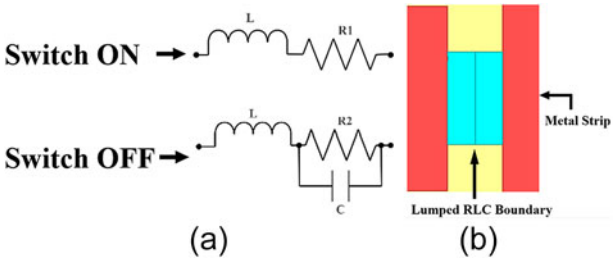

Figure 3. (a) Equivalent circuit of PIN diode and (b) PIN diode model.

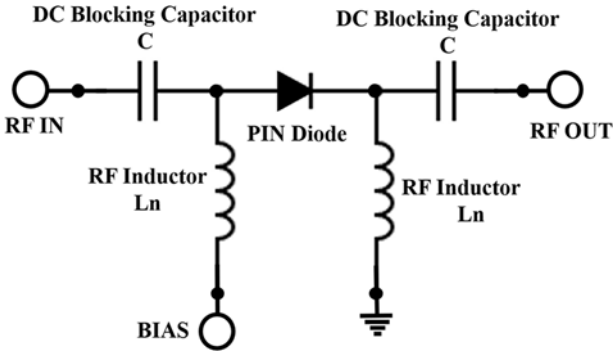

Figure 4. RF PIN diode used to create a series switch.

borders of the regular patch. The Koch curve has drawn a lot of interest within the fractal curve categories because of its simple generation procedure. Here, the asymmetric Koch fractal curves are used to produce two orthogonal modes of similar amplitude for CP radiation along the patch boundaries [15] and [20]. Figure 2 displays the antenna prototype top and side different points of view. The center of the hexagonal ring patch is filled with a smaller-dimensional Koch fractal element.

Effect of all of the composed iterations

The operating band is directly impacted by fractal geometry that is incorporated into a patch design. The antenna shape is first modelled as a regular hexagonal patch in antenna 1, and then the hexagonal-structured slot is etched from the patch's middle portion in antenna 2. Furthermore, a second iteration of the Koch curve-based fractal is carried out along the patch element's inner portion in the antenna construction. Figure 6 shows the 0^{th}, 1^{st}, and 2^{nd} order of iterations of the Koch curve fractal structure. From Figs. 7 and 8, it is observed that, as the number of iterations increases, the depth of operating frequency/axial ratio (AR) band of the radiator increases with a broad frequency range covering 3–7.91/3.33–7.14 GHz but realized gain of the radiator is slightly affected.

https://doi.org/10.1017/S1759078724001302 Published online by Cambridge University Press

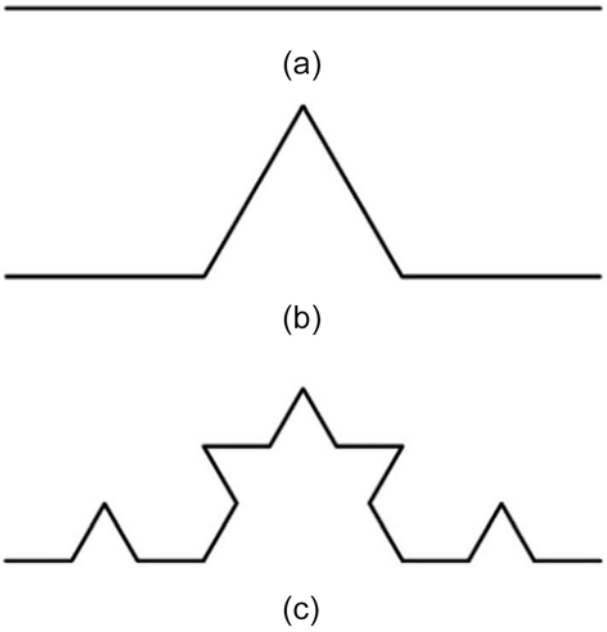

Figure 5. Koch curve iterations: (a) 0th, (b) 1st, and (c) 2nd order [20].

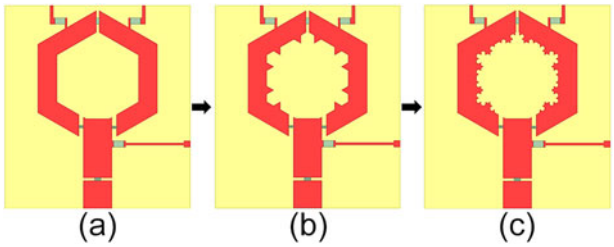

Figure 6. Different stages of reconfigurable fractal antenna.

Effect of the added extensions

The stages of the evolution of the proposed antenna are depicted in Fig. 9. Their matching performances are displayed in Fig. 10. Two orthogonal modes are formed by the gaps generated by the diodes' position, which perturbs the electric field [15]. These modes provide CP over 3.33–7.14 GHz. But $|S_{11}|$ is higher than −10 dB. The ground plane represented by Ant. 2 has a slit cut in it with a length of L_f to enhance impedance matching. In Ant. 3, the CP bandwidth is widened by a triangular extension in the ground plane on the right. Consequently, CP bandwidth is significantly enhanced. The dip of AR is shifted and a new dip is created at 6.2 GHz by a second triangular extension on the left. Hence, the CP bandwidth is increased to 3.33–7.14 GHz. The realized gain in the overall band of the antenna increases after cutting the slit and adding left/right triangular extensions to the ground plane, as shown in the Figs. 9 and 10. Initially it is about 2 dBi but after implementing various stages in the antenna, it increased to 5.07 dBi in the operational band. In this case, D_1 is turned off and D_2 is turned on for all simulations [8, 10, 20–22, 35–37].

It is obvious by the above that the ring's rotating current components are what primarily produce the CP. When D_1 is ON and D_2 is OFF, it produces LHCP in the $+z$ direction shown in Fig. 11. RHCP is obtained when the current rotates in the opposite direction shown in Fig. 12 and the diode conditions are inverted, that is, D_1 is ON and D_2 is OFF. In a similar manner, two CP modes combine to produce LP when both diodes are ON.

Effect of ground length L_e

As seen in Fig. 1(c), the parameter L_e indicates the length of the partial ground. Figure 13 illustrates how various L_e values affect the outcome. The length L_e is reduced, the IBW at S_{11} less than −10 dB with wideband is achieved. When the length, L_e, decreases, the reflection coefficient at higher resonant frequencies is decreased.

Effect of rectangular slit length L_f in the ground

The effect of rectangular slot length (L_f) of the antenna on the reflection coefficient (S_{11}) is studied in order to obtain better performance. In Fig. 14, several values of L_f are shown and compared with other values of rectangular slit placed slightly behind the feed on the ground plane when both the switches D_1 and D_2 are in state 2 (OFF, ON). An impedance match is created by the addition of a rectangular slit, and coupling between the patch and ground plane occurs. The length (L_f) of the slot is expanded by 1 mm while the slot width (W_f) remains same. The S_{11} below −20 dB at 3.5 and 7 GHz rises gradually as L_f increases, as seen in Fig. 14. According to the simulated results, $L_f = 4.5$ mm has a better return loss than other L_f values because of better impedance matching.

Proposed antenna performance and discussion

The measurement setup is shown in Fig. 15. Figure 16 displays the measured and simulated reflection coefficient ($|S_{11}| < -10$ dB) for each of the three polarization states. The S_{11} for the CP mode is consistently less than −10 dB between 3 and 7.91 GHz. 3.54–6.75 GHz is the comparable value for the LP mode. A rectangular horn antenna with excellent linear polarization purity is used as the source antenna in the experimental setup depicted in Fig. 15 in order to measure the phase of the two field components with respect to the signal generator. Because rectangular horn antennas produce less cross-polarization over wide bandwidths than circular polarized feeds, a significant source of measurement error is consequently eliminated. The antenna far-field radiation pattern in each cut (Φ) is generated by plotting the parameters Θ (deg), P_{RHCP} (dB), and P_{LHCP} (dB). A practical antenna normally generates a desired reference polarization in addition to an undesirable cross-polar component, which is polarized in the opposite hand. For example, in Fig. 6, RHCP is the reference polarization, and LHCP is the cross-polar component. In the main beam, $|\, P_{\mathrm{RHCP}}\ (\mathrm{dB}) - P_{\mathrm{LHCP}}\ (\mathrm{dB})\,|$ gives the cross-polar level at a given azimuth angle Θ. For a perfectly circularly polarized pattern, this level is $-\infty$ dB (AR = 0 dB), and for a LP field, where the two CP signals are of identical magnitude, this level is 0 dB (AR = ∞ dB). The reference and cross-polar spatial patterns can also be retrieved from an AR plot, which is generated using a LP spinning source antenna in the experimental setup. To obtain this data, the antenna under test must be moved in azimuth (Θ) and the source horn must be constantly rotated about its axis (Φ). The ripples in the radiation pattern are a consequence of the beam ellipticity, which occurs when a finite cross-polar component exists. The AR is defined by the depth of the nulls, and

https://doi.org/10.1017/S1759078724001302 Published online by Cambridge University Press

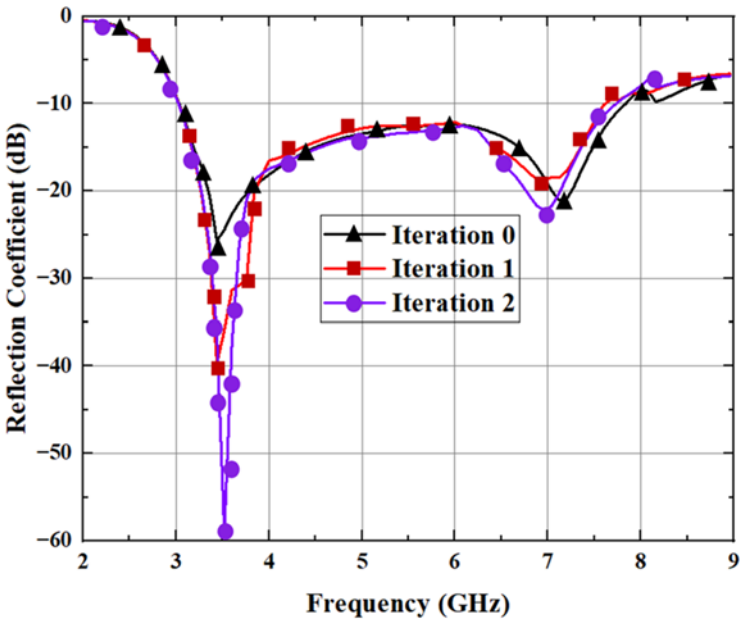

Figure 7. S_{11} plot for different stages of the antenna.

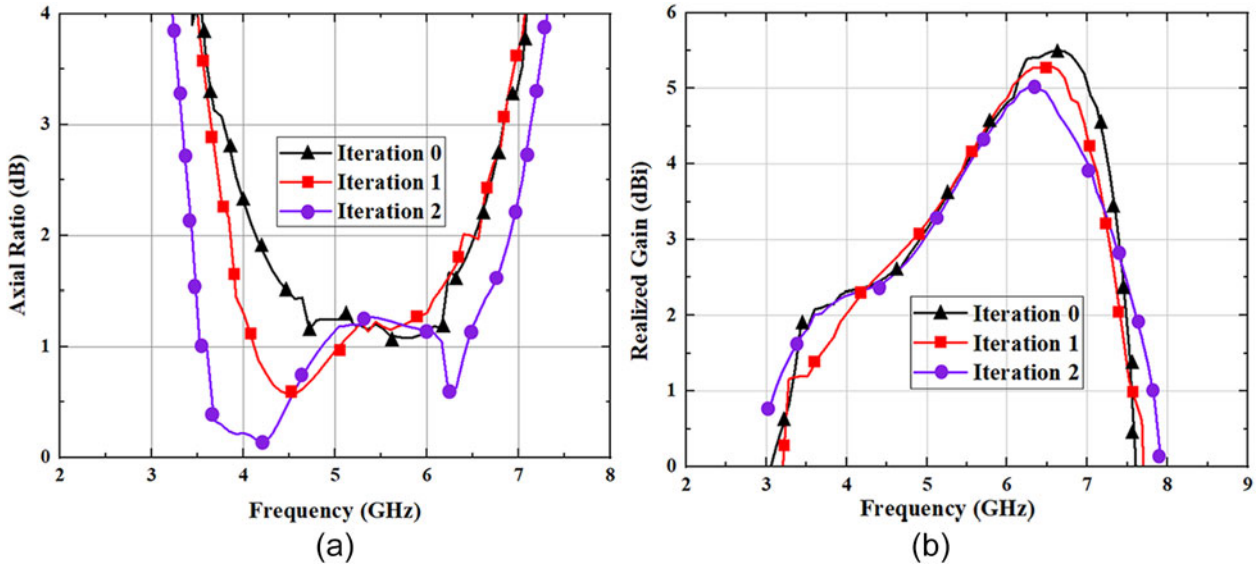

Figure 8. (a) Axial ratio and (b) realized gain plot for different stages of the antenna.

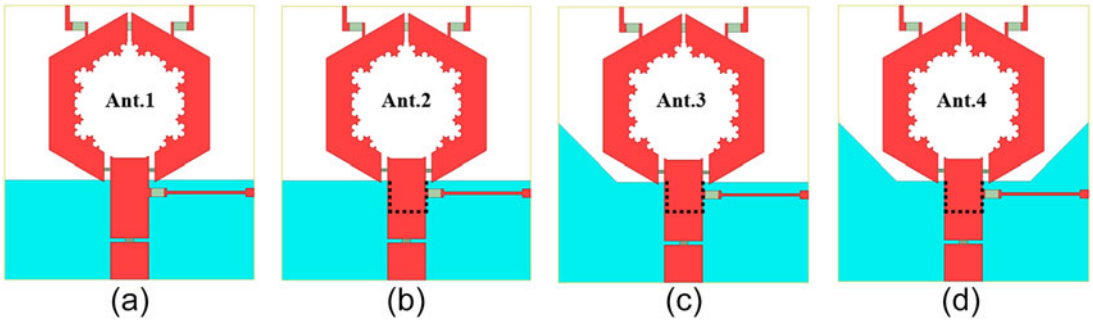

Figure 9. Different stages of antenna.

https://doi.org/10.1017/S1759078724001302 Published online by Cambridge University Press

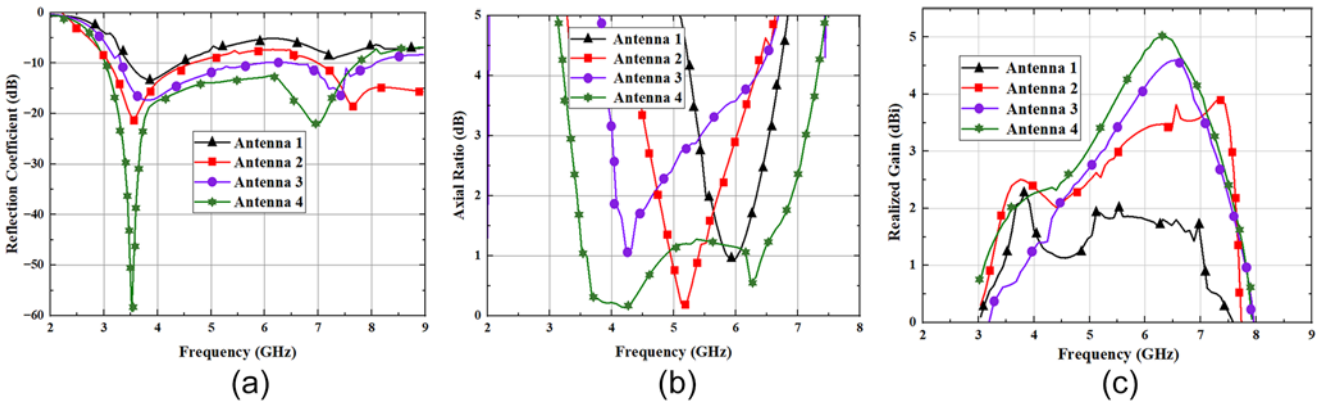

Figure 10. (a) Reflection coefficient (S_{11}), (b) axial ratio, and (c) realized gain plot for different stages of the antenna.

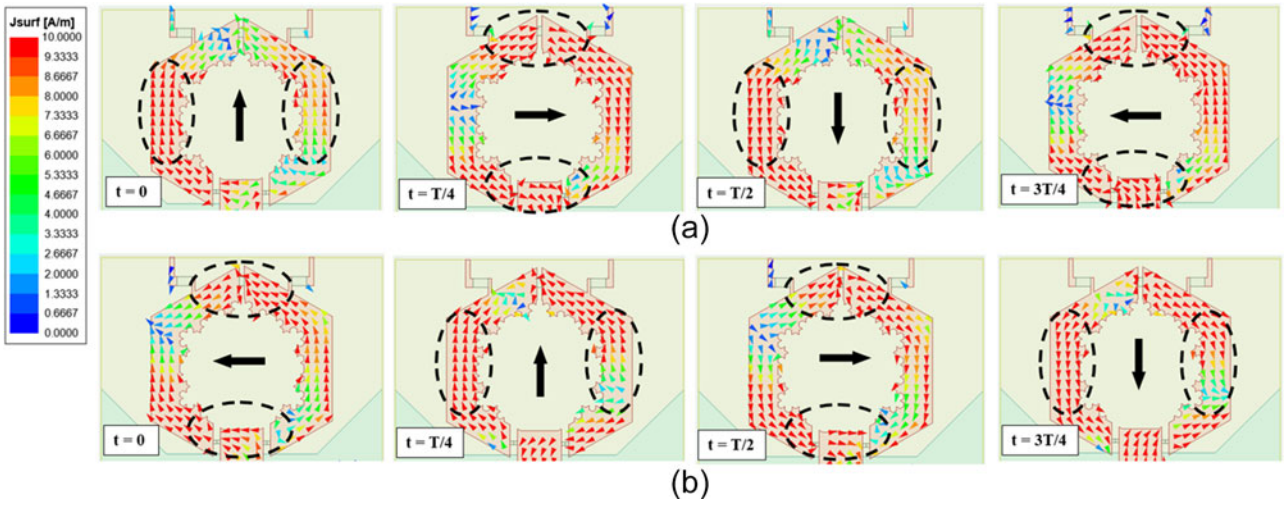

Figure 11. Surface current distribution of proposed hybrid reconfigurable fractal antenna for Case I (a) at 4.4 GHz (b) at 6.2 GHz.

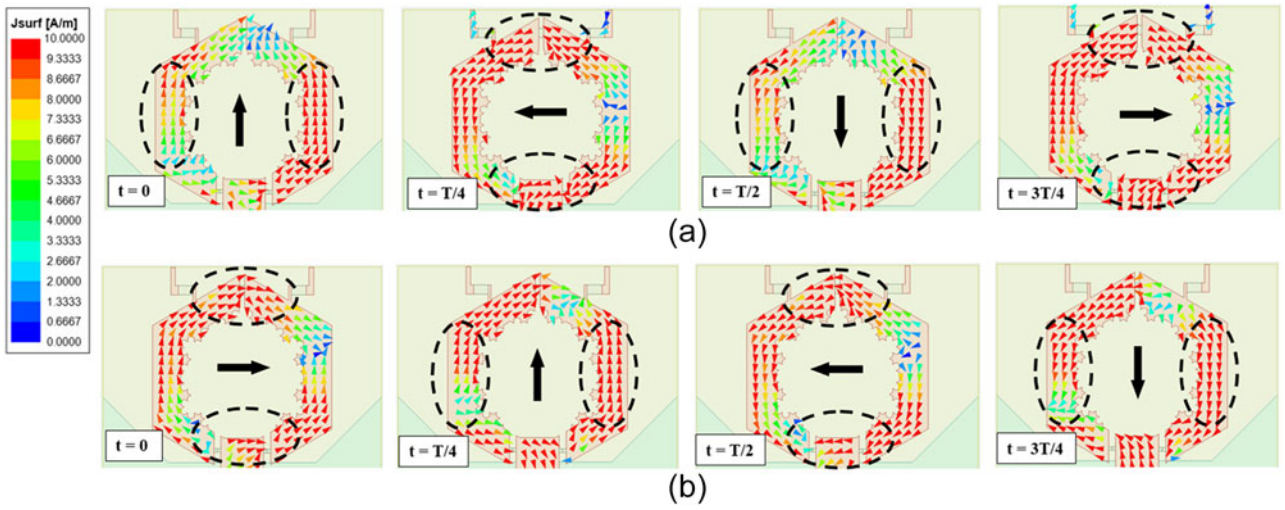

Figure 12. Surface current distribution of proposed hybrid reconfigurable fractal antenna Case II (a) at 4.4 GHz (b) at 6.2 GHz.

https://doi.org/10.1017/S1759078724001302 Published online by Cambridge University Press

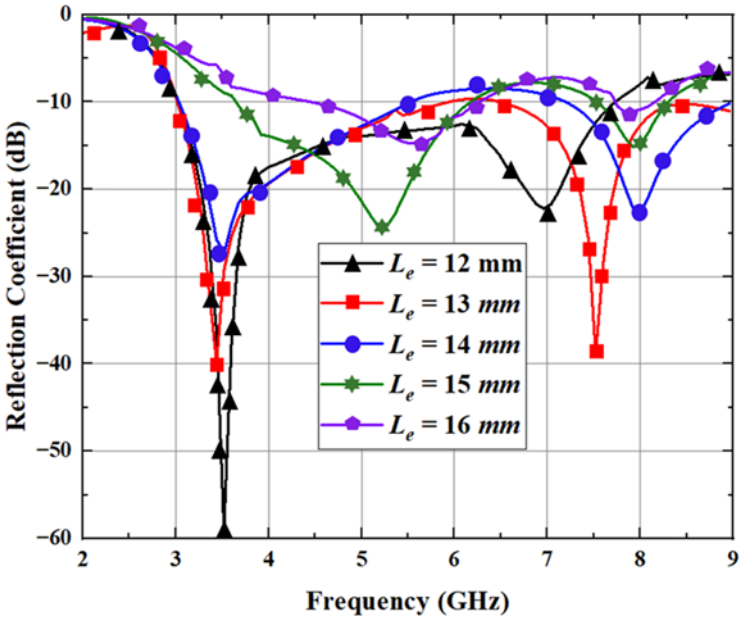

Figure 13. Reflection coefficient (S_{11}) plot for different cases of the antenna.

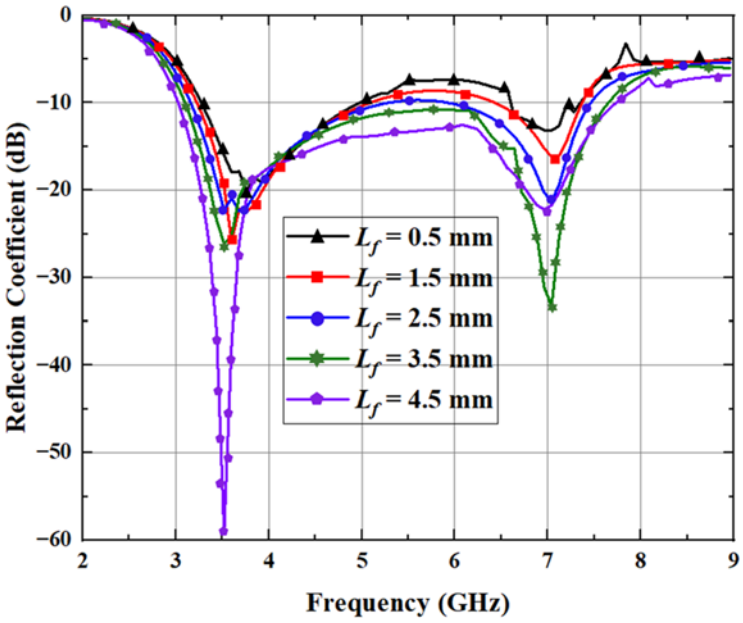

Figure 14. Reflection coefficient (S_{11}) plot for different cases of the antenna.

it is related to the cross-polarization provided by the formula (5) [27, 30–32].

$$\mathrm{AR} = 20\log_{10}\left(\frac{1+e}{1-e}\right) \tag{5}$$

where $e = 10^{-P_{dB}/20}$and P_{dB} is the cross-polar power.

The simulated and measured AR for the LHCP and RHCP modes, respectively, is below 3 dB over 3.6–6.9 GHz (62.86%) and 3.33–7.14 GHz (72.78%), as illustrated in Fig. 17. A minor discrepancy between the simulated and measured observations is noticed due to differences in the diode characteristics that are utilized for polarization reconfigurability. Figure 18 displays the measured broadside gain variations. The radiation efficiency of the antenna is analyzed in simulation and measurement mode as shown in Fig. 19. Proposed design achieves radiation efficiencies 94.8/95.9/95.6 and 94.9/97/94.2 (in percentage) during simulation and experimental process in LP/LHCP/RHCP polarization state, respectively. Figures 20 and 21 display the normalized far-field radiation patterns at 4.6 GHz for the CP states, respectively. The sense of polarization is considered in +z direction. The −z direction shows the opposite of it. The difference between the co-polarization and cross-polarization levels is consistently 18.5 dB. Figure 22 displays the radiation patterns for LP. Table 1 provides a summary of the polarization states and corresponding diode states.

The proposed antenna and a few recently published wide-band RFAs are compared in Table 2. The switching element of the antenna shown in references [7, 10], and [22–24] is positioned inside the radiating element or signal path and requires a sophisticated biasing network in order to switch. With a large total CP bandwidth, the proposed antenna has a good profile. The dual-band antenna mentioned in reference [23] has performance

https://doi.org/10.1017/S1759078724001302 Published online by Cambridge University Press

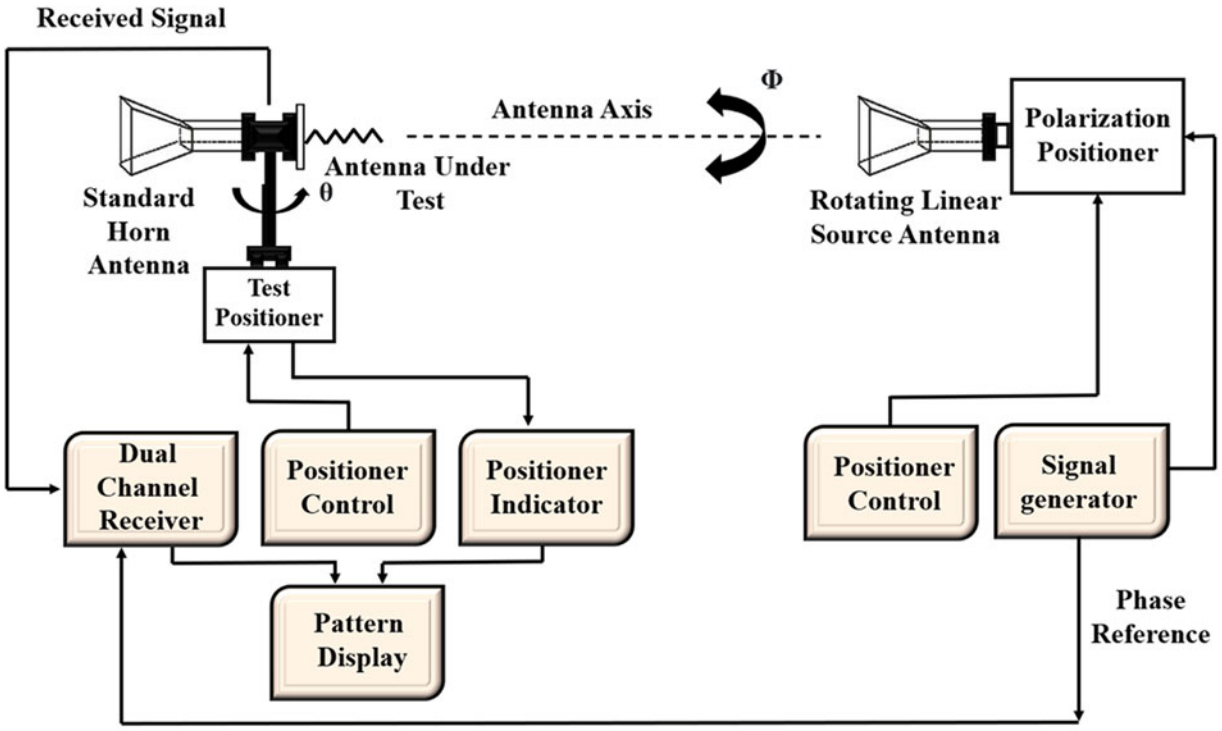

(a)

(b)

Figure 15. Measurement setup of the proposed RFA antenna.

that is comparable to that of the proposed design, but it is larger and has a switching element inside the RF signal line. Although the narrow band radiator in reference [24] has a low gain, it is larger in size and has a lower overlapping CP bandwidth than the proposed antenna. In Table 2, few selected designs are having low ARBW. Larger sizes are yet another significant disadvantage of these radiators. On the other hand, the proposed design operates in different polarization states, wide IBW and compact in size. This illustrates the benefits of the RFA above previous comparable works. The majority of antennas intended for reconfigurability will have complex design and multiple no. of switching elements. However, the designed antenna uses the fewest possible switching

https://doi.org/10.1017/S1759078724001302 Published online by Cambridge University Press

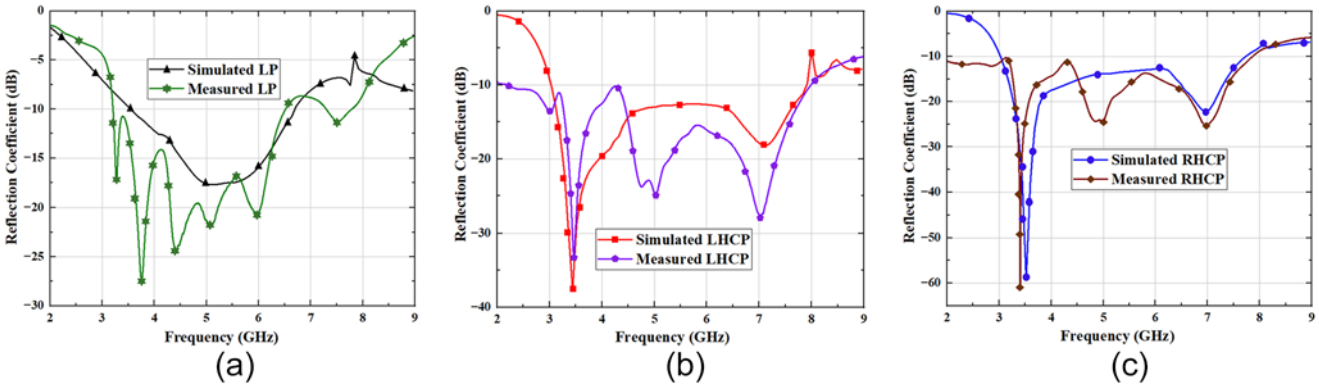

Figure 16. S_{11} plot for different cases of the antenna.

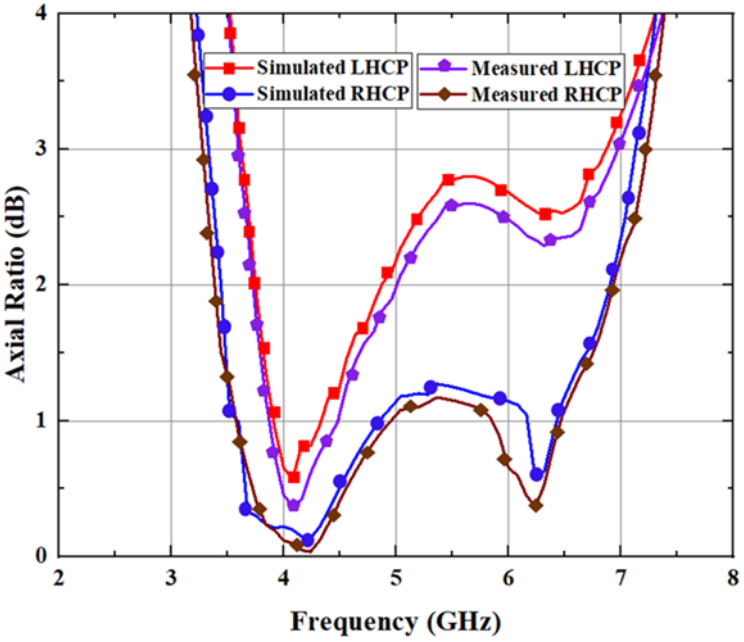

Figure 17. Axial ratio plot for different cases of the antenna.

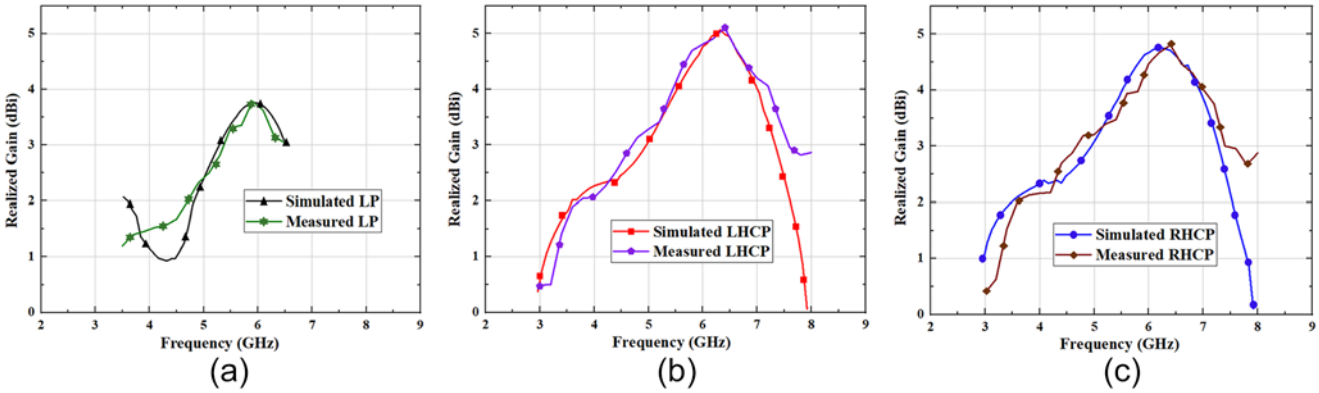

Figure 18. Realized gain plot for different cases of the antenna.

https://doi.org/10.1017/S1759078724001302 Published online by Cambridge University Press

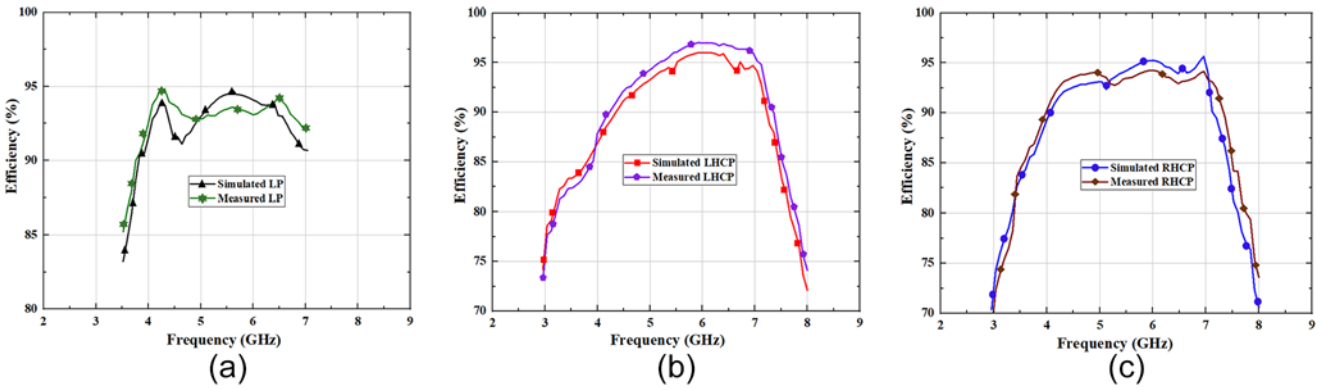

Figure 19. Efficiency plot for different cases of the antenna.

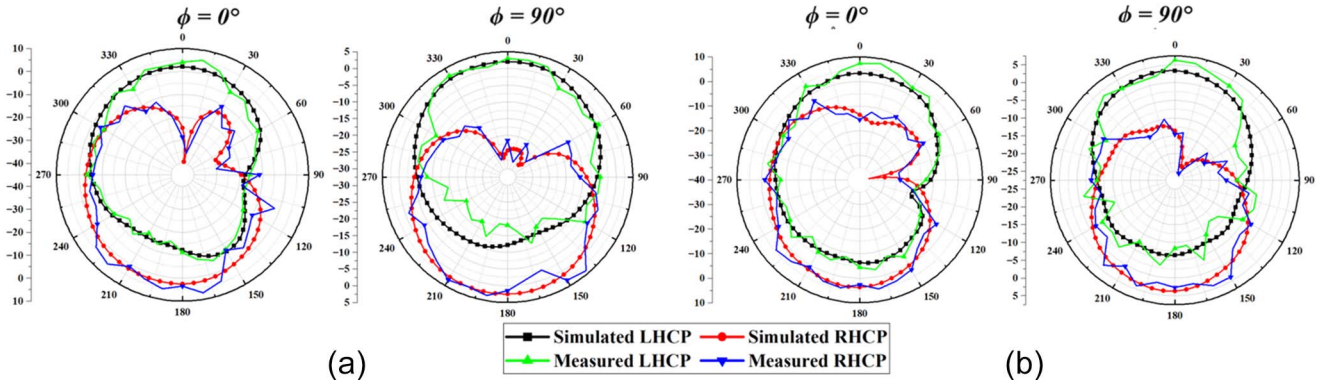

Figure 20. Radiation patterns of the antenna when D_1 is ON and D_2 is OFF (LHCP) (a) at 4.2 GHz and (b) at 5.2 GHz.

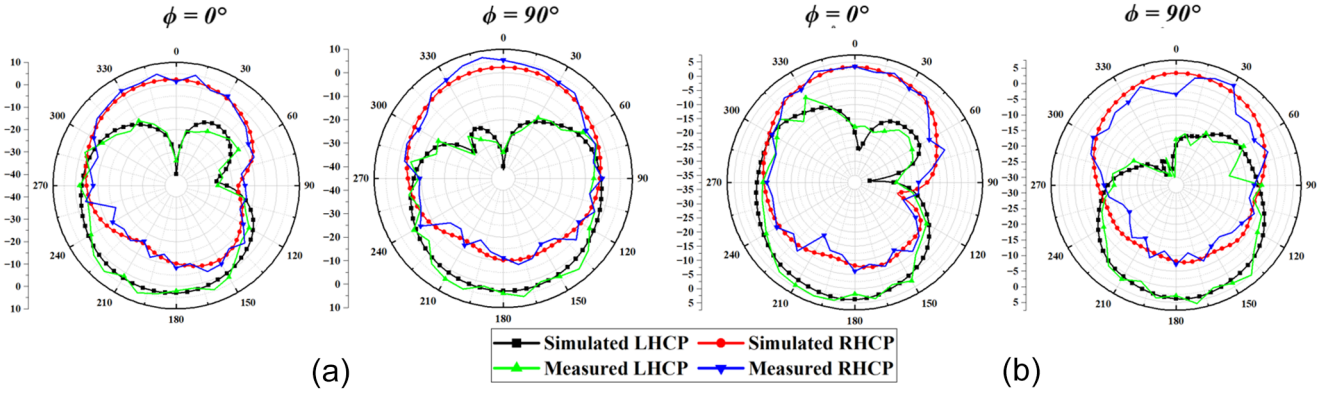

Figure 21. Radiation patterns of the antenna when D_1 is OFF and D_2 is ON (RHCP) (a) at 4.2 GHz and (b) at 5.2 GHz.

components. The primary goal of this research is polarization reconfiguration of antenna for wireless applications. The significant gain at the operating frequency bands is provided by the antenna. The antenna covers a wide range of application bands, and polarization reconfiguration are offered by applying two PIN diodes. The designed structure is distinguished because it is compact in dimensions, has a good substrate material (Rogers RT Duroid), and has a peak realized gain of 5 dBi across the whole realized gain compared to other structures. Table 2 shows that the proposed fractal radiator has a high gain, small dimension, and better polarization reconfiguration performance, making it suitable for wireless communication services.

https://doi.org/10.1017/S1759078724001302 Published online by Cambridge University Press

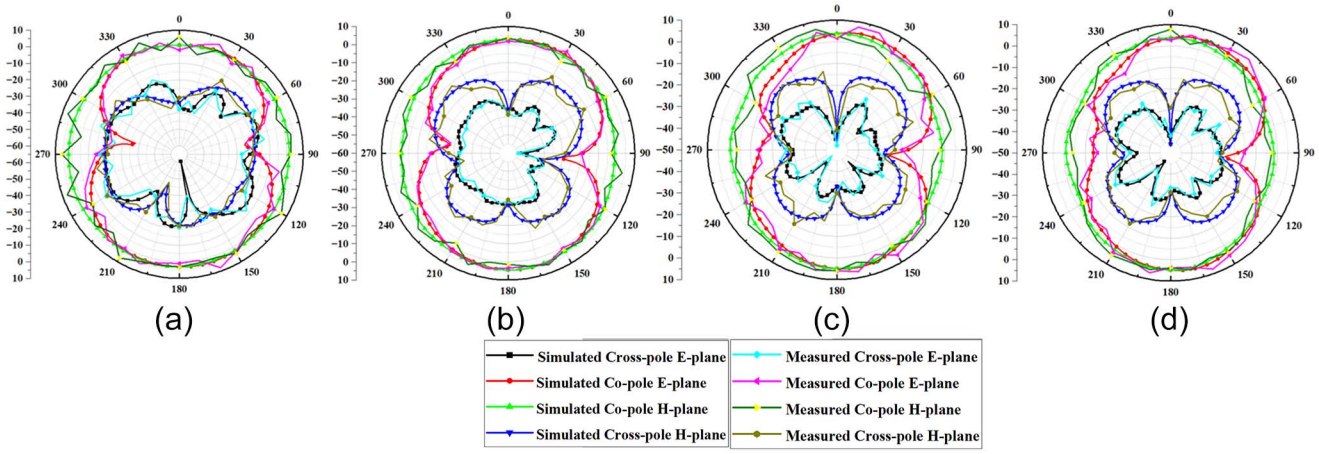

Figure 22. Radiation patterns at (a) 4.4, (b) 5.2, (c) 5.8, and (d) 6 GHz.

Table 1. Operation modes of the proposed wideband polarization reconfigurable antenna (PRA)

Diode D_1	Diode D_2	Pol. state	IBW (GHz)	ARBW (GHz)	Overlapped BW (GHz)	Peak realized gain (dBi)
ON	OFF	LHCP	3–7.91 (90%)	3.6–6.9 (62.86%)	3.6–6.9	4.75
OFF	ON	RHCP	3–7.73 (88.16%)	3.33–7.14 (72.78%)	3.33–7.14	5.07
ON	ON	LP	3.54–6.7 (61.7%)	–	–	3.8

Table 2. Performance comparison of the designed geometry with existing works

Ref.	Antenna geometry	Dimensions (mm^3)	Type of reconfiguration	Type of switch	No. of switches	Type of substrate	IBW (GHz)	ARBW (GHz)	Peak realized gain (dBi)	Application
[7]	Minkowski island fractal	40 × 40 × 1.6	Dual band polarization	PIN	4	TLY–5 (2.2)	15.44% (2.33–2.72 GHz) 13.16% (2.98–3.40 GHz)	17.61% (2.2–2.62 GHz) 8.69% (2.91–3.18 GHz)	10.5	Wireless applications
[8]	Fan shaped slot	–	RHCP LHCP	PIN	2	–	18.2 (LHCP) 16.7 (RHCP) 8.7 (LP)	3.7(LHCP) 3.2 (RHCP)	10.6	Advanced wireless communication systems
[9]	Rectangular path	35.2 × 67.5 × 1.52	RHCP LHCP	PIN	2	Taconic substrate 3.5	%1.91 −4.0 GHz (70%), 2.00–2.52 GHz (23%) (RHCP), 2.10–2.54 GHz (19%) (LHCP)	2.34 to 2.46 GHz (4.5%) RHCP, 4.4% (2.33–2.44 GHz) LHCP	1.2, 0.6, 0.5 (RHCP, LHCP, and LP)	WLAN applications
[10]	Straight dipoles	–	RHCP LHCP	PIN	12	Taconic RF–35(3.5)	2.34–2.48	2.34–2.48 GHz, 2.42–2.48 GHz	6.7	WLAN applications
[12]	U-slot microstrip patch	40 × 40 × 3.175	Polarization	PIN	2	RT/Duroid 5880 2.2	5.6–6.3, 5.72 - 6.08 (CP, LP)	2.8%	6.3–7.5 dBic, 6.25–7.3 dBi (CP, LP)	WLAN applications
[13]	C-shaped slotted circular patch	–	HP, VP, LHCP, RHCP	PIN	2	Roger RT Duroid 5870 (2.33)	20% (2.16–2.64), 25.6% (2.21–2.86)	(4%),	8, 7	Wireless applications

(*Continued*)

https://doi.org/10.1017/S1759078724001302 Published online by Cambridge University Press

Table 2. (*Continued.*)

Ref.	Antenna geometry	Dimensions (mm^3)	Type of reconfiguration	Type of switch	No. of switches	Type of substrate	IBW (GHz)	ARBW (GHz)	Peak realized gain (dBi)	Application
[14]	Square patch, a T-shaped feed	70 × 70 × 1.6	Polarization	PIN	2	FR–4 4.4	11.3% (2.43–2.72 GHz),	2.27% (2.615–2.67 GHz),	7.26	Wireless and satellite communication applications
[15]	Koch fractal boundary patch	48 × 48 × 3.2	Polarization	PIN	4	Roger RT Duroid 5880 (2.2)	2.4% (2450–2510 MHz), 1.1% (2467–2493 MHz), 3.8% (1766–1834 MHz) and 1.6% (1786–1814 MHz),	1.2% and 0.9%	–	GSM/Wi-Fi application bands
[22]	Rectangular shaped element	34.5 × 28 × 1.6	Polarization	PIN	8	FR–4 4.4	3.12–4.63, 5.06–6.07	3.38–3.65, 5.01–5.95	1.11,0.91	Cognitive radio and MIMO system
[23]	Fractal-shaped slot-ring array	83 × 83 × 31	Polarization	PIN	32	Roger RT Duroid 5880 (2.2)	2–4, 4–8	2–4, 4–8	5.7, 11.5	S–C band
[24]	Circular fractal geometry	65 × 65 × 1.6	Polarization	PIN	4	FR–4 4.4	2.36–2.48	2.38–2.41 (LHCP), 2.38–2.40 (RHCP)	3.26 (LHCP), 3.12 (RHCP)	ISM (Industrial, scientific, and medical) band
Proposed work	**Koch fractal patch**	**33 × 30 × 1.6**	**Polarization**	**PIN**	**2**	**Roger RT Duroid 5880 (2.2)**	**3–7.91 (LHCP), 3–7.73 (RHCP), 3.54–6.7 (LP)**	**3.6–6.9 (LHCP), 3.33–7.14 (RHCP)**	**4.75, 5.07, 3.8**	**S and C-band applications**

Conclusion

A low-cost printed polarization reconfiguration monopole antenna is designed for wireless applications. Two PIN diodes are utilized to generate LP, RHCP, or LHCP characteristics. The connection between the diodes and the radiating element has the least impact on the radiation characteristics. It contains three measured frequency bands: 3.54–6.7 GHz for Case I, 3.91–7.91 GHz for Case II, and 3.73–7.73 GHz for Case III. Thus, from 3 to 7.91 GHz, the proposed antenna's IBW offers continuous wideband frequency coverage. For the LHCP modes (Case I) and RHCP modes (Case II), the simulated AR is below 3 dB over 3.6–6.9 GHz and 3.33–7.14 GHz, respectively. 3.54–6.7 GHz is the corresponding value for the LP mode (Case III). A peak realized gain of 4.75, 5.07, and 3.8 dBi is achieved at 6.2, 6.3, and 6 GHz for Case I, Case II, and Case III, respectively. The proposed antenna is simple to construct and has a simple layout. Because of its simple geometry and less complicated bias design, it is feasible and easy to utilize. The proposed antenna has good polarization reconfigurable features, according to simulation and experimental data. There is no need for extra switching elements when designing a big array antenna due to the simple topology of the offered antenna. It is applicable to a wide range of high-speed wireless system applications such as cognitive radio, ISM band, and satellite communication system. This work can realize the design of hybrid mode (frequency, polarization, and pattern) or other parameters at the same time with various techniques such as artificial magnetic conductor (AMC), electromagnetic band-gap (EBG), metamaterial, defected ground structure (DGS)/fractal defected ground structure (FDGS) to enhance antenna performances. This compound antenna element can also be designed antenna arrays in order to satisfy the multitask detection requirements in radar detections, satellite communications, etc.

Author contributions. All authors contributed equally to analyzing data and reaching conclusions, and in writing the paper.

Funding statement. This research received no specific grant from any funding agency, commercial or not-for-profit sectors.

Competing interests. The authors report no conflict of interest.

References

1. **Mamta NV** (2024) Frequency reconfigurable circular microstrip G-slotted antenna with DGS for various wireless applications. *International Journal of Microwave and Wireless Technologies* **16**(3), 1–10. doi:10.1017/S1759078724000242
2. **Li T, Zhai H, Wang X, Li L and Liang C** (2015) Frequency-reconfigurable bow-tie antenna for Bluetooth, WiMAX, and WLAN applications. *IEEE*

Antennas and Wireless Propagation Letters **14**, 17–174. doi:10.1109/LAWP.2014.2359199

3. **Reji V and Manimegalai CT** (2023) Light controlled frequency reconfigurable antenna for wireless applications. *International Journal of Microwave and Wireless Technologies* **15**(1), 143–149. doi:10.1017/S1759078722000137
4. **Kumar R, Singh S, Singh C and Pal A** (2022) Multiband antenna design based on Gosper fractal for implantable biomedical devices. *International Journal of Microwave and Wireless Technologies* **14**(8), 970–980. doi:10.1017/S1759078721001203
5. **Ezzahry B, Elhamadi T-E, Lasalle M and Touhami NA** (2023) New method based on genetic algorithm and Minkowski fractal for multiband antenna designs. *International Journal of Microwave and Wireless Technologies* 1–12. doi:10.1017/S1759078723001071
6. **Hao ZC, Fan KK and Wang H** (2017) A planar polarization-reconfigurable antenna. *IEEE Transactions on Antennas and Propagation* **65**(4), 1624–1632. doi:10.1109/TAP.2017.2670440
7. **Saraswat K and Harish AR** (2020) Dual-band polarisation reconfigurable grounded fractal slot antenna. *IET Microwaves, Antennas & Propagation* **14**(14), 1786–1790. doi:10.1049/iet-map.2020.0542
8. **Chen Q, Li JY, Yang G, Cao B and Zhang Z** (2019) A polarization-reconfigurable high-gain microstrip antenna. *IEEE Transactions on Antennas and Propagation* **67**(5), 3461–3466. doi:10.1109/TAP.2019.2902750
9. **Panahi A, Bao XL, Yang K, O'Conchubhair O and Ammann MJ** (2015) A simple polarization reconfigurable printed monopole antenna. *IEEE Transactions on Antennas and Propagation* **63**(11), 5129–5134. doi:10.1109/TAP.2015.2474745
10. **Li QY, Tran HH and Park HC** (2018) Reconfigurable antenna with multiple linear and circular polarization diversity for WLAN applications. *Microwave and Optical Technology* **60**(12), 2893–2899. doi:10.1002/mop.31411
11. **Bhattacharjee A, Dwari S and Mandal MK** (2019) Polarization-reconfigurable compact monopole antenna with wide effective bandwidth. *IEEE Antennas and Wireless Propagation Letters* **18**(5), 1041–1045. doi:10.1109/LAWP.2019.2908661
12. **Qin PY, Weily AR, Guo YJ and Liang CH** (2010) Polarization reconfigurable U-slot patch antenna. *IEEE Transactions on Antennas and Propagation* **58**(10), 3383–3388. doi:10.1109/TAP.2010.2055808
13. **Mak KM, Lai HW, Luk K and Ho KL** (2017) Polarization reconfigurable circular patch antenna with a C-shaped. *IEEE Transactions on Antennas and Propagation* **65**(3), 1388–1392. doi:10.1109/TAP.2016.2640141
14. **Lee SW and J SY** (2016) Simple polarization-reconfigurable antenna with T-shaped feed. *IEEE Antennas and Wireless Propagation Letters* **15**, 114–117. doi:10.1109/LAWP.2015.2432462
15. **Reddy VV and Sarma NVSN** (2015) Circularly polarized frequency reconfigurable Koch antenna for GSM/Wi-Fi applications. *Microwave and Optical Technology Letters* **57**(12), 2895–2898. doi:10.1002/mop.29463
16. **Poonam T and Falguni R** (2020) Fork-shaped frequency and pattern reconfigurable antenna. *International Journal of Communication Systems* **33**(17), 1–11. doi:10.1002/dac.4613
17. **Chandra KV, Satyanarayana M and Battula KT** (2020) A novel miniature hexagonal shape switched pattern and frequency reconfigurable antenna. *International Journal of Communication Systems* **33**(5), 1–8. doi:10.1002/dac.4264
18. **Jose MC, Chithra D, Sreeja R, S. B, Meraline S and Radha S** (2019) A novel wideband pattern reconfigurable antenna using switchable parasitic stubs. *Microwave and Optical Technology Letters* **61**(4), 1090–1096. doi:10.1002/mop.31698
19. **Jin GP, Li ML, Xu YC, Yang J and Liao SW** (2020) Differentially fed six-beam switchable reconfigurable antenna. *IET Microwaves, Antennas & Propagation* **14**(7), 573–577. doi:10.1049/iet-map.2019.0622
20. **Pandav S, Sadhukhan G, Das TK, Behera SK and Mohanty M** (2022) Circularly polarized high gain Koch fractal antenna for space applications. *Sādhanā* **47**(4), 276. doi:10.1007/s12046-022-02047-2
21. **Darimireddy NK, Reddy RR and Prasad AM** (2018) A miniaturized hexagonal-triangular fractal antenna for wide-band applications [antenna applications corner]. *IEEE Antennas and Propagation Magazine* **60**(2), 104–110. doi:10.1109/MAP.2018.2796441
22. **Bhattacharjee A and Dwari S** (2021) A monopole antenna with reconfigurable circular polarization and pattern tilting ability in two switchable wide frequency bands. *IEEE Antennas and Wireless Propagation Letters* **20**(9), 1661–1665. doi:10.1109/LAWP.2021.3092345
23. **Huang J, Shirazi M and Gong X** (2022) A new arraying technique for band-switchable and polarization-reconfigurable antenna arrays with wide bandwidth. *IEEE Open Journal of Antennas and Propagation* **3**, 1025–1040. doi:10.1109/OJAP.2022.3201617
24. **Das TK, Das R, Kumar A, Kumari R, Mandal P, Mukhi RK and Pradhan JD** (2023) Modified fractal-based polarization-reconfigurable patch antenna for 2.4 GHz ISM band applications. *International Conference on Wireless Communications Signal Processing and Networking (WiSPNET)*, 01–05. 10.1109/WiSPNET57748.2023.10134042
25. **Patel K and Behera SK** (2023) A miniaturized wideband fractal antenna combining Sierpinski and Minkowski fractals. In *3rd International Conference on Range Technology (ICORT)*, 1–4. 10.1109/ICORT56052.2023.10249058
26. **Patel K and Behera SK** (2023) Design of frequency reconfigurable hybrid fractal antenna for wireless applications. In *IEEE Microwaves, Antennas, and Propagation Conference (MAPCON) Ahmedabad*, India, 1–5. doi: 10.1109/MAPCON58678.2023.10463919
27. **Balanis CA** (2015) *Microstrip Antennas. Antenna Theory: Analysis and Design*, 3rd edn. John Wiley & Sons.
28. https://cdn.macom.com/datasheets/MADP-000907-14020x.pdf
29. **Bhattacharjee A and Dwari S** (2021) Wideband monopole antenna with circular polarization reconfigurability and pattern diversity. In *2021 IEEE Indian Conference on Antennas and Propagation (InCAP)*, Jaipur, Rajasthan, India, 957–960. doi: 10.1109/InCAP52216.2021.9726343
30. **Toh BY, Cahill R and Fusco VF** (2003) Understanding and measuring circular polarization. *IEEE Transactions on Education* **46**(3), 313–318. doi:10.1109/TE.2003.813519
31. **Patel K, Pandav S and Behera SK** (2024) Reconfigurable fractal devices. *IEEE Microwave Magazine* **25**(7), 41–62. doi:10.1109/MMM.2024.3387037
32. **Patel K and Behera SK** (2023) Design of Koch curve-based fractal antenna for ultra-wideband applications. In *2023 IEEE Microwaves, Antennas, and Propagation Conference (MAPCON)*, Ahmedabad, India, 1–5. doi: 10.1109/MAPCON58678.2023.10464044
33. https://search.murata.co.jp/Ceramy/image/img/P02/JELF243A-9139.pdf
34. https://docs.rs-online.com/663d/A700000008615923.pdf
35. **Abdelgwad AH** (2018) Microstrip patch antenna enhancement techniques. *International Scholarly and Scientific Research and Innovation* **12**(10), 703–710.
36. **Akinola S, Hashimu I and Singh G** (2019) Gain and bandwidth enhancement techniques of microstrip antenna: A technical review. In *2019 International Conference on Computational Intelligence and Knowledge Economy (ICCIKE)*, Dubai, United Arab Emirates, 175–180. doi: 10.1109/ICCIKE47802.2019.9004278
37. **Kumar A, Gupta N and Gautam PC** (2016) Gain and bandwidth enhancement techniques in microstrip patch antennas - A review. *International Journal of Computer Applications* **148**(7), 9–14. doi:10.5120/ijca2016911207

Khushbu Patel received the Bachelor of Engineering (B.E.) degree in Electronics Engineering from Madhav Institute of Technology and Science (MITS), Gwalior, India in 2018 and the Master of Engineering (M.E.) degree in Electronics and Telecommunication Engineering from Jabalpur Engineering College (JEC), Jabalpur, India in 2021. She is currently pursuing a Ph. D. degree in Microwave Engineering Specialization from National Institute of Technology (NIT) Rourkela, Rourkela, India. Her areas of interest are planar antennas, reconfigurable fractal antennas, and antenna arrays.

https://doi.org/10.1017/S1759078724001302 Published online by Cambridge University Press

Santanu Kumar Behera received the B.Sc. (Eng.) degree in Electronics and Telecommunication Engineering from Veer Surendra Sai University of Technology (VSSUT) Burla, Sambalpur, India, in 1990, and the M.E. degree in Electronics and Telecommunication Engineering and the Ph.D. degree (Engg.) from Jadavpur University Kolkata, India, in 2001 and 2008, respectively. He is currently a Professor in the Department of Electronics and Communication Engineering, National Institute of Technology Rourkela, India. His areas of interest are Electromagnetic theory, Planar antennas, Dielectric Resonator antennas, Fractal antennas, Reconfigurable antennas, and Radio Frequency Identification (RFID) systems. Dr. Behera is an Associate Editor-in-Chief of the ACES Journal.

https://doi.org/10.1017/S1759078724001302 Published online by Cambridge University Press